Corrosion Science 54 (2012) 193–200

Contents lists available at SciVerse ScienceDirect

Corrosion Science

journal homepage: www.elsevier.com/locate/corsci

# Investigation on the inhibition behavior of a pentaerythritol glycoside for carbon steel in 3.5% NaCl saturated $Ca(OH)_2$ solution

Xin Zhou [a,b], Huaiyu Yang [a,*], Fuhui Wang [a]

[a] State Key Laboratory for Corrosion and Protection, Institute of Metal Research, Chinese Academy of Sciences, Wencui Road 62, Shenyang 110016, China
[b] Department of Metallurgic Engineering, Liaoning Institute of Science and Technology, 42 Wenhua Road, Benxi 117022, China

ARTICLE INFO

*Article history:*
Received 15 March 2011
Accepted 11 September 2011
Available online 17 September 2011

*Keywords:*
A. Steel reinforced concrete
B. EIS
B. XPS
C. Alkaline corrosion

ABSTRACT

A pentaerythritol glycoside (PG) was synthesized and then its corrosion inhibition for carbon steel in 3.5% NaCl saturated $Ca(OH)_2$ solution was investigated using potentiodynamic polarization, electrochemical impedance spectroscopy (EIS), as well as atomic force microscopy (AFM) and X-ray photoelectron spectroscopy (XPS). Results indicated that the PG compound acted as an anodic inhibitor by strong chemical interaction with the carbon steel surface according to the Langmuir adsorption isotherm. The inhibition efficiency and pitting potential on carbon steel increased with increasing concentrations of the inhibitor. Zero charge potential measurements and quantum chemical calculations provided insight into the inhibition mechanism, which are discussed.



## 1. Introduction

The surfaces of steel rebars embedded in concrete structures are usually in a passive state due to the presence of a thin oxide film formed in high alkaline concrete conditions. However, when passivity is destroyed by aggressive ions, especially chloride ions, and by the pH reduction of concrete pore solution as a result of concrete carbonation, steel reinforcements may suffer corrosion attack. The most common corrosion form is the pitting corrosion of reinforcement because of localized breakdown of the passive film on steel surfaces caused by chloride ions [1–3]. In order to prevent or mitigate the reinforcement corrosion, several approaches are proposed in literatures. Among available methods, the use of corrosion inhibitor seems to be a promising method because of its easy application and low cost compared with other preventive methods [4–6].

Nowadays, there are a number of inhibitors commercially available. Generally, they are based on the inorganic compounds such as nitrites, sodium mono-fluoro-phosphate, and the mixtures of some organic compounds such as alkanolamines, organic amines and fatty acid esters [1,7]. However, some of them are not authorized to use in some European countries due to their possible toxicity and worse inhibition effect in case of insufficient dosage [8,9]. Therefore, it is necessary to develop environmental-friendly corrosion inhibitors to replace inorganic salts either partially or totally. This term requires that the components used as inhibitors should not be toxic to mankind and have low environmental impact and optimal biodegradability, while possess high inhibition efficiency and reasonable cost. In recent years, hence, more and more interests have been given to the study of new organic compounds that are able to prevent or stop the corrosion of reinforcements in concrete structures, as well as to the understanding of their inhibition mechanism [6,10–15]. Existing data suggest that most of the organic compounds used as corrosion inhibitors can adsorb on metal surfaces via heteroatom such as nitrogen, sulfur, oxygen, phosphorus and multiple bonds or aromatic rings, subsequently blocking the active sites on the metal surfaces and decreasing the corrosion rates of metals [16–19]. The inhibition effects of organic inhibitors mainly depend on their affinity and compatibility to the metal surface [18].

Alkyl glycosides have been widely used in consumer goods such as foods, cosmetics and pharmaceuticals due to their favorable surface activity in aqueous media and ecological properties (for instance, biodegradable performance), and also their easy preparation from many renewable raw materials such as carbohydrates and long hydrocarbon chain alcohols [20–22]. Therefore, they have been extensively studied in recent years not only out of fundamental research interests, but also because of their diverse practical applications [23–25]. Nevertheless, it needs to be pointed out that, up to our knowledge, few works have been reported in the literature in which glycosides were studied as inhibitors to protect metals against corrosion in various aggressive media, and there is very little information available on the understanding of their inhibition mechanism.

In the present paper, a pentaerythritol glycoside (labeled as PG and shown in Fig. 1) has been synthesized to investigate its inhibition effect on the corrosion of carbon steel in 3.5% NaCl saturated $Ca(OH)_2$ solution by different electrochemical techniques. Atomic

* Corresponding author. Tel.: +86 24 23915899; fax: +86 24 23893624.
*E-mail address:* hyyang@imr.ac.cn (H. Yang).

0010-938X/$ - see front matter © 2011 Elsevier Ltd. All rights reserved.
doi:10.1016/j.corsci.2011.09.018

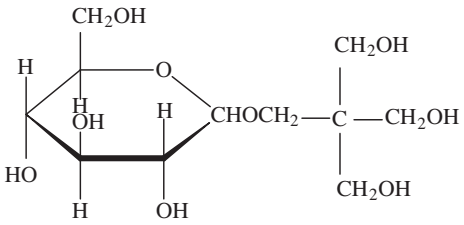


**Fig. 1.** Molecular structure of the tested inhibitor.

force microscopy was used to examine the changes of the carbon steel surfaces corroded in test solutions with and without the inhibitor. X-ray photoelectron spectroscopy was performed to verify the presence of the inhibitor on the carbon steel surface. These results are interpreted in terms of the physiochemical interactions between the adsorbed inhibitor molecules and the carbon steel surfaces. Zero charge potential measurements together with quantum chemical calculations were further employed to provide additional insight into the inhibition mechanism of such an inhibitor in an alkaline chloride medium.

## 2. Experimental

### 2.1. Synthesis of PG

A mixture of anhydrous glucose and pentaerythritol was heated to 90 °C, then phosphoric acid (in the amount of 1.5% (mass%) of the glucose) was added as a catalyst; the mixture was continuously heated to 120–130 °C and then kept at this temperature for 1.25 h. When the solution was cooled to 90 °C, the reacted mixture was neutralized by a saturated NaOH solution to a pH of 7–8, and the resulting compound (PG) was obtained. A complete description about synthetic processes was described elsewhere [26]. The compound structure was confirmed by FT-IR spectroscopy.

Fig. 2 shows the FT-IR spectrum of the synthesized compound. The peaks at 2948 and 2890 $cm^{-1}$ were ascribed to $CH_2$ stretching vibrations and the peak at 1484 $cm^{-1}$ was assigned to the stretching vibration of C—H [27]. The band at 1463 $cm^{-1}$ was attributed to the C—C stretching vibration and the C—O stretching vibration was found in the region 1070–1140 $cm^{-1}$ [28]. These spectrum data indicated that the target compound PG has been synthesized.

### 2.2. Test solution

The test solution used in all experiments was a 3.5% NaCl saturated $Ca(OH)_2$ solution (pH 12.5) prepared from reagent grade chemicals and bi-distilled water. A water bath was used to keep the solution at 25 °C during the entire testing period.

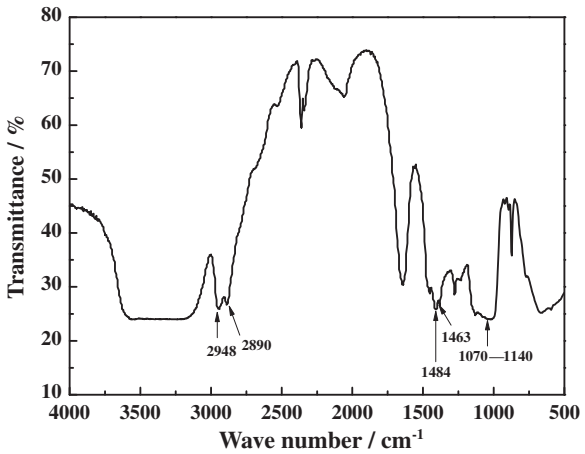


**Fig. 2.** FT-IR spectrum of PG.

### 2.3. Materials

Working electrodes ($\Phi 10 \times 2$ mm) were cut from the carbon steel bar with a composition (in mass%): C, 0.15; Si, 0.15; Mn, 0.44; P, 0.30; S, 0.03; and Fe in balance, and then connected to a copper wire and embedded in an epoxy resin leaving an exposed working area of 0.785 $cm^2$. Before testing, the working electrodes were ground gradually with grit SiC paper (grade 240, 400, 600 and 800), then degreased in acetone and ultrasonically cleaned in alcohol.

### 2.4. Electrochemical measurements

Electrochemical experiments were carried out using Parstat 2273 (Princeton Applied Research). A conventional three-electrode cell was used, equipped with a saturated calomel electrode (SCE) as the reference electrode and a large platinum plate as the counter electrode. All electrochemical measurements were conducted after the working electrodes were immersed in test solutions with and without the addition of an inhibitor for 0.5 h. Electrochemical impedance spectroscopy was performed in the frequency range of 100 kHz–10 mHz with an amplitude of 10 mV peak-to-peak, using AC signals at the open circuit potential (OCP). Potentiodynamic polarization curves were measured from −150 mV versus OCP to the potential at which the anodic current density increased abruptly with a scan rate of 1 mV $s^{-1}$. The potentiodynamic polarization and EIS data were analyzed by means of $C_{view}$ and $Z_{view}$ software, respectively. All potentials reported in the paper were referred to SCE.

### 2.5. Surface morphological observation and analysis

In order to observe any changes in surface morphologies of the carbon steel samples after testing, the specimens were first immersed in the test media with and without an inhibitor for 0.5 h, then cleaned with bi-distilled water and acetone, and dried with cool air. Then the morphology of the tested sample was observed by atomic force microscopy (AFM, Pico Plus 2500). The scanning area in the images was 5000 × 5000 nm.

For evaluating the surface composition and obtaining information on the surface coverage of the inhibitor, carbon steel samples were immersed in the working electrolytes with and without an inhibitor respectively for 0.5 h, and then their surfaces were analyzed by X-ray photoelectron spectroscopy (XPS, ESCALAB 250, VG Company) under pressures below $5.5 \times 10^{-8}$ mbar, using a monochromatic Al Kα (1486.6 eV) radiation source. The binding energies were referenced to adventitious carbon (284.8 eV). The collected XPS data were processed with XPSPEAK Version 4.1 software for Shirley background subtraction, fitting and peak deconvolution.

## 3. Results and discussion

### 3.1. Electrochemical measurements

#### 3.1.1. Potentiodynamic polarization

Fig. 3 depicts typical polarization curves for carbon steel in 3.5% NaCl saturated $Ca(OH)_2$ solution in the absence and presence of an inhibitor. It can be seen that the anodic process of carbon steel corrosion in alkaline chloride solution was effectively retarded by the inhibitor, and this effect became more pronounced with increasing inhibitor concentrations, while the cathodic corrosion current densities were reduced after the addition of an inhibitor. These results

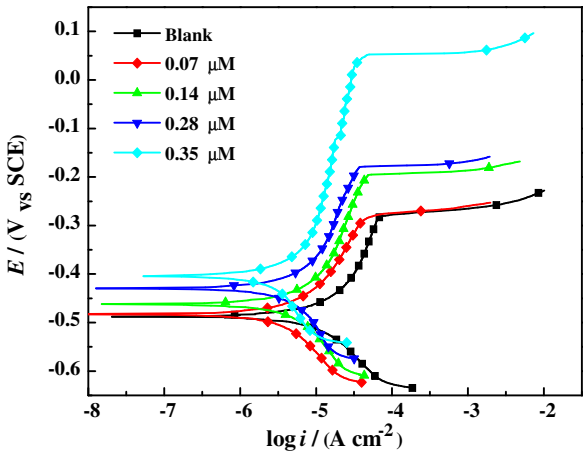


**Fig. 3.** Potentiodynamic polarization curves for carbon steel in 3.5% NaCl sat. $Ca(OH)_2$ solutions without and with different concentrations of the inhibitor.

suggest that the inhibitor has a stronger inhibition effect on the anodic dissolution of iron than the cathodic reduction of oxygen via strongly suppressing the anodic oxidation of iron. This corrosion inhibition for carbon steel in alkaline chloride solution can be attributed to the covering of adsorbed inhibitor molecules on the carbon steel surface.

It also can be seen that after the addition of the inhibitor, the anodic polarization curves showed a significant shift of the pitting potential in positive direction and a wider passive region in comparison with that in the blank solution, while the addition of the inhibitor remarkably decreased the corrosion current density. These results reveal that the pitting corrosion was strongly suppressed by the inhibitor. Fig. 4 shows the values of pitting potential of carbon steel in test solutions with different concentrations of the inhibitor, where the pitting potential ($E_{pit}$) was defined as the potential at which the anodic current density started to increase rapidly and a dashed line indicates the pitting potential ($E^0_{pit}$) measured in the blank solution. It is evident that the pitting potential increased with increasing concentrations of the inhibitor, suggesting that the chloride-induced corrosion on the carbon steel surface was suppressed by the inhibitor. This effect can be ascribed to the outcome of a competitive adsorption on the electrode surface between the inhibitor molecules and the chloride ions. In other words, the adsorbed inhibitor molecules on the carbon steel surface can effectively screen the potential sites for the chloride ion adsorption and then act as a

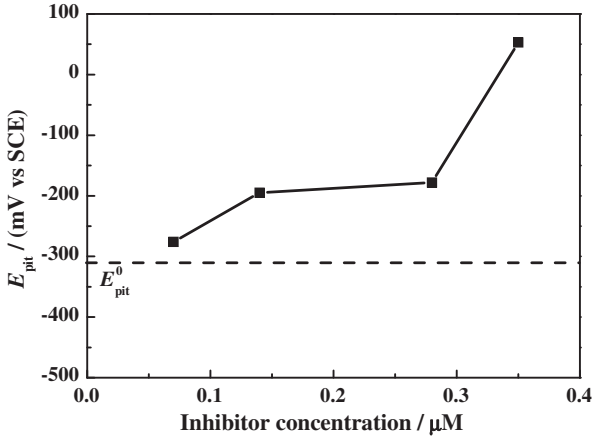


**Fig. 4.** Pitting potential values of carbon steel in 3.5% NaCl sat. $Ca(OH)_2$ solutions with different concentrations of the inhibitor. A dashed line represents the pitting potential in blank solution.

barrier to block the adsorption of chloride ions onto metal surfaces [10,29,30]. This situation will force chloride ions to interact with the less energetically favorable sites on carbon steel surface, thereby requiring greater activation energy for pitting to occur. Hence, in the presence of an inhibitor, it is necessary to move the electrode potential to more positive values to initially favor the adsorption of the chloride ions and then to drive them access to the carbon steel surface for the occurrence of pitting corrosion, ultimately leading to an increase in the pitting potential of carbon steel. Similar results were also reported for most other tested organic compounds [29–32].

Table 1 summarizes some of the associated corrosion electrochemical parameters such as the corrosion potential ($E_{corr}$), the cathodic ($\beta_c$) and anodic ($\beta_a$) slops obtained by fitting the polarization data in the vicinity of $E_{corr}$ ±100 mV. As can be seen from Table 1, there is a definite positive shift in $E_{corr}$ values with increasing concentrations of the inhibitor, indicating that the compound behaved as an anodic inhibitor [33].

### 3.1.2. Electrochemical impedance

Fig. 5 shows the Nyquist (a) and Bode (b) plots for carbon steel in 3.5% NaCl saturated $Ca(OH)_2$ solutions with and without an inhibitor at OCP. It can be observed that the impedance response of the electrode has significantly changed after the addition of an inhibitor in the blank solution. In comparison with the blank solution, in the presence of an inhibitor, the diameters of the semi-circles in Nyquist plots increased with increasing inhibitor concentrations, and the low frequency limit of the impedance in Bode plot was more than half an order of magnitude greater than that in the blank solution when the inhibitor concentration was 0.35 μM. These results indicate that the impedance of the carbon steel electrode increased with increasing concentrations of the inhibitor, consequently resulting in an increase in the inhibition effect, and that the carbon steel corrosion was effectively retarded due to the forming of a protective film on the electrode surface. In addition, the impedance spectra did not present perfect semicircles, this phenomenon can be attributed to the frequency dispersion [34,35].

It is also evident that the Nyquist plots are composed of two slightly depressed capacitive loops, the one at high frequencies can be attributed to the charge transfer resistance ($R_{ct}$), which could correspond to the resistance between the carbon steel surface and the outer Helmholtz plane [36]. The other one at low frequencies is related to the film resistance ($R_f$), which can be ascribed to the adsorbed inhibitor molecules and all other accumulated kinds [37]. So the impedance measurement results can be explained by the equivalent circuit shown in Fig. 6. In this equivalent circuit, $R_s$ represents the solution resistance, $R_{ct}$ is the charge transfer resistance, $R_f$ represents the film resistance. Taking into account the inhomogeneity at the solid/liquid interface [38], the constant phase elements $CPE_1$ and $CPE_2$ are used to replace the double layer capacitance ($C_{dl}$) and the film capacitance ($C_f$), respectively. The fitted electrochemical parameters are listed in Table 2, where the inhibition efficiency ($\eta$) was calculated by the following equation:

$$\eta\% = \frac{R_{ct} - R^0_{ct}}{R_{ct}} \times 100 \quad (1)$$

**Table 1**
The electrochemical parameters estimated from polarization data for carbon steel in 3.5% NaCl saturated $Ca(OH)_2$ solution with different concentrations of the inhibitor.

| Conc. (μM) | $E_{corr}$ (mV/SCE) | $-\beta_c$ (mV dec$^{-1}$) | $\beta_a$ (mV dec$^{-1}$) |
|---|---|---|---|
| Blank | −486 | 81 | 79 |
| 0.07 | −475 | 96 | 85 |
| 0.14 | −462 | 103 | 95 |
| 0.28 | −434 | 122 | 100 |
| 0.35 | −402 | 144 | 104 |

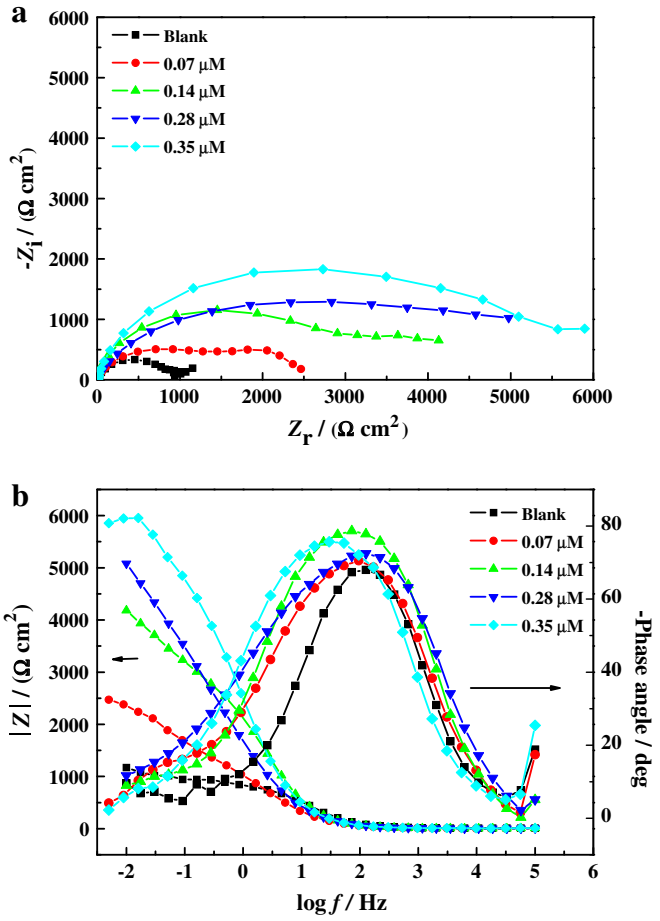


**Fig. 5.** Nyquist (a) and Bode (b) plots for carbon steel in 3.5% NaCl sat. $Ca(OH)_2$ solutions without and with different concentrations of the inhibitor.

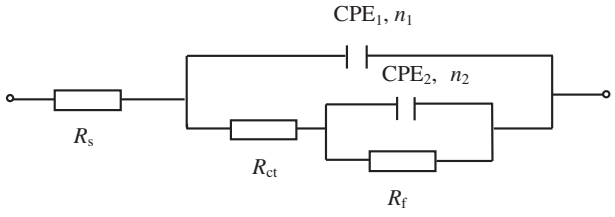


**Fig. 6.** The equivalent circuit used to simulate the impedance data.

where $R_{ct}^0$ and $R_{ct}$ are the charge transfer resistances in the uninhibited and the inhibited solution, respectively.

It is apparent from Table 2 that by increasing concentrations of the inhibitor, the $C_{dl}$ and $C_f$ values tended to decrease, whereas the

**Table 2**
The fitted electrochemical parameters from EIS for carbon steel in 3.5% NaCl saturated $Ca(OH)_2$ solution with different concentrations of the inhibitor.

| Conc. (μM) | Blank | 0.07 | 0.14 | 0.28 | 0.35 |
|---|---|---|---|---|---|
| $R_s$ (Ω cm$^2$) | 10.7 | 4.9 | 4.8 | 4.2 | 4.0 |
| $C_{dl}$ (μF cm$^{-2}$) | 238.1 | 166.3 | 116.1 | 47.4 | 29.1 |
| $n_1$ | 0.90 | 0.87 | 0.84 | 0.85 | 0.90 |
| $R_{ct}$ (Ω cm$^2$) | 581 | 1959 | 2568 | 3351 | 5692 |
| $C_f$ (μF cm$^{-2}$) | 2733.0 | 694.0 | 32.3 | 31.1 | 29.2 |
| $n_2$ | 0.65 | 0.74 | 0.94 | 0.92 | 0.86 |
| $R_f$ (Ω cm$^2$) | 1591 | 2157 | 2186 | 6468 | 8051 |
| $\eta$ (%) | | 70.3 | 77.4 | 82.7 | 89.8 |
| $\theta$ | | 0.70 | 0.77 | 0.83 | 0.898 |

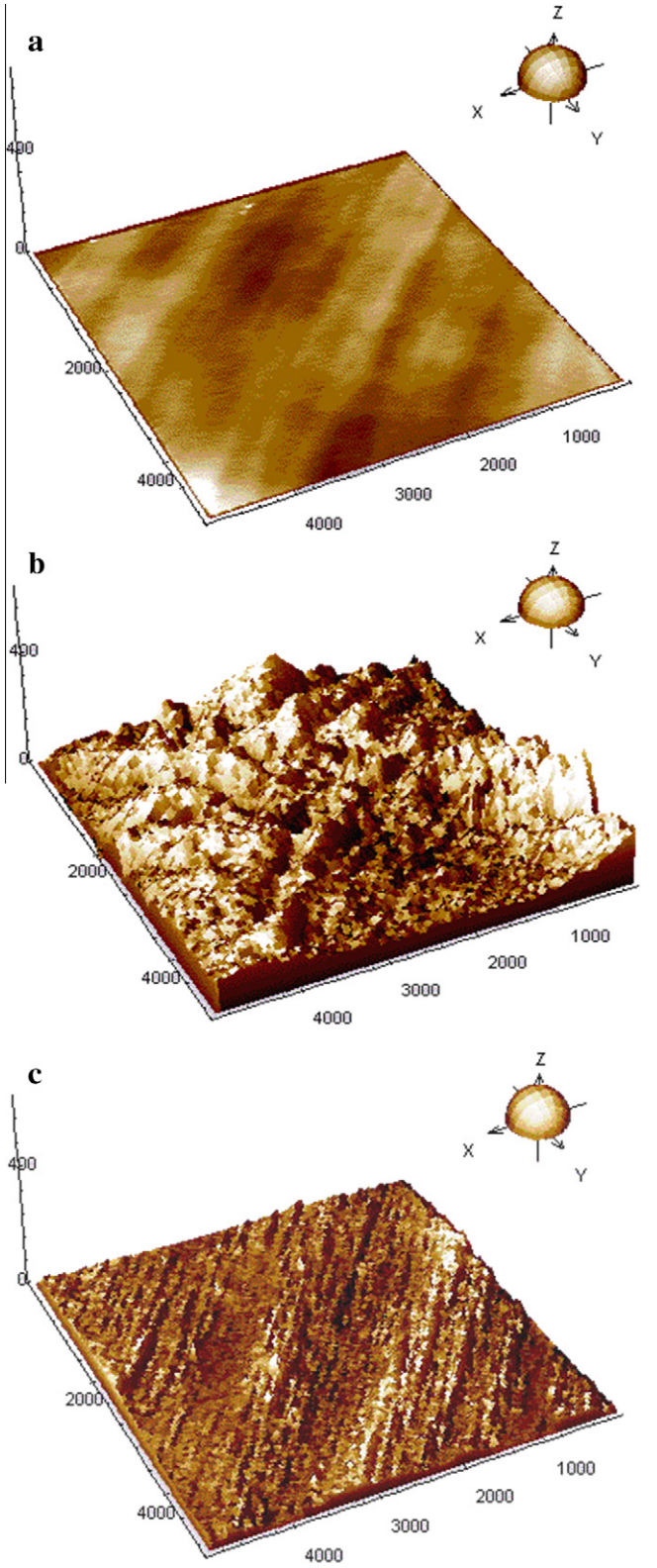


**Fig. 7.** AFM three-dimensional images for carbon steel specimens immersed in 3.5% NaCl sat. $Ca(OH)_2$ solution: (a) before immersion, (b) without the inhibitor, (c) with 0.28 μM inhibitor.

$R_{ct}$ and $R_f$ values increased. The significant decrease in the capacitance values can be ascribed to a decrease in the dielectric constant or an increase in the double electric layer thickness due to the adsorption of the inhibitor molecule on the carbon steel surface [39]. The remarkable increase in $R_{ct}$ suggests that the amount of

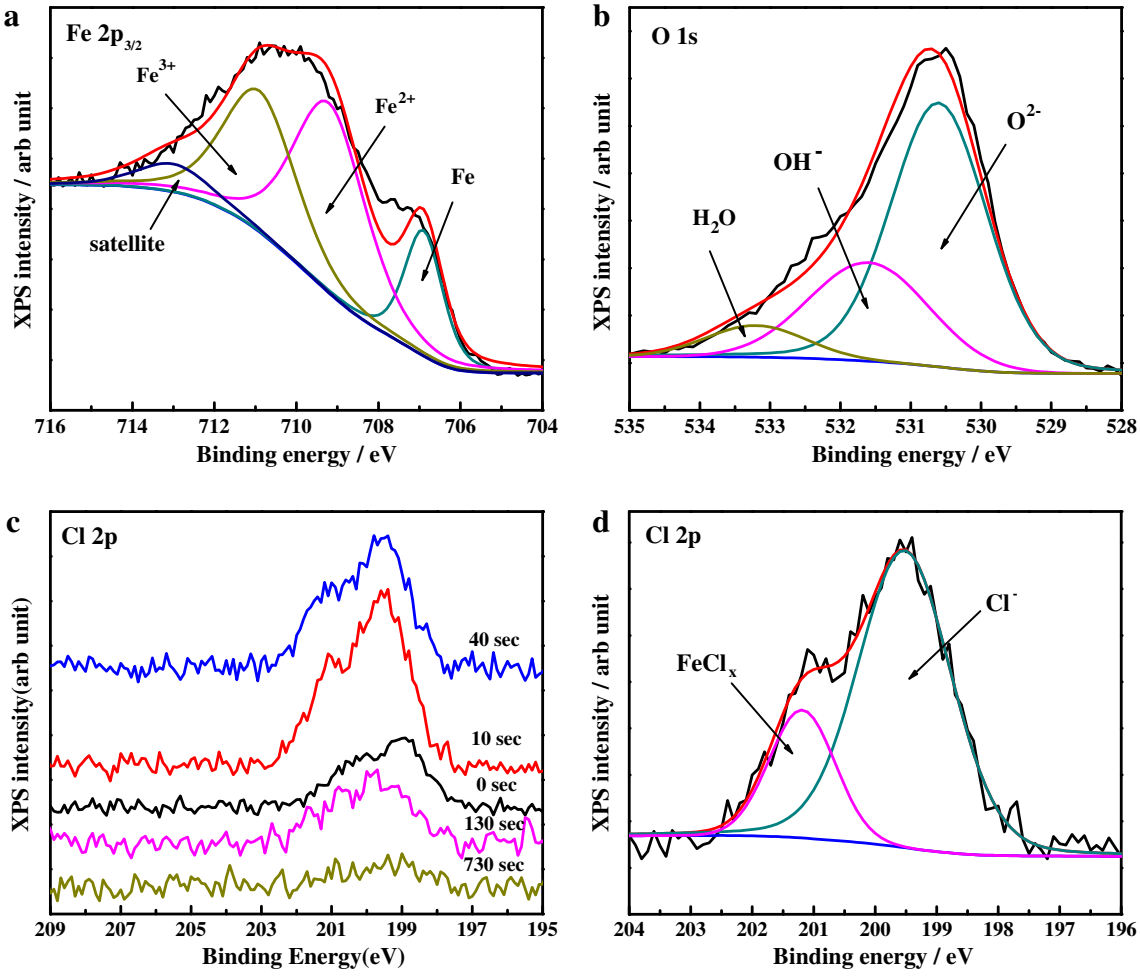


**Fig. 8.** XPS spectra for carbon steel samples exposed to 3.5% NaCl sat. $Ca(OH)_2$ solution for 0.5 h at the OCP; (a) Fe $2p_{3/2}$; (b) O 1s; (c) the depth profile spectra of Cl 2p; (d) the deconvoluted profile spectra for Cl 2p after 10 s sputtering.

inhibitor molecules adsorbed on the carbon steel surface increases and consequently results in the decreasing of active sites necessary for the coupled dissolution reaction. As to the increasing of $R_f$, it could be the result of film formation consisting of adsorbed inhibitor molecules and/or corrosion products on the carbon steel surface, thereby increasing the pitting potential and strongly hindering the chloride-induced localized corrosion [5,6,10,40,41].

### 3.2. Surface morphological observation and analysis

#### 3.2.1. AFM observation

3D AFM images for the carbon steel samples after 0.5 h immersion in 3.5% NaCl saturated $Ca(OH)_2$ solutions with and without 0.28 μM inhibitor are depicted in Fig. 7. It can be observed that the carbon steel sample in the blank solution suffered from obvious corrosion and the sample surface is rougher than that in the solution with inhibitor. Through calculation, the mean roughness of the carbon steel surface exposed to the blank solution is about 108.18 nm, as a result of the chloride attack, meanwhile in the presence of the inhibitor, the mean roughness decreases to 27.38 nm, as a consequence of inhibitor adsorption on the steel surface.

#### 3.2.2. X-ray photoelectron spectroscopy

Figs. 8 and 9 show the profiles of spectra for Fe, O, Cl and C on the carbon steel surfaces after 0.5 h immersion in test solutions with and without 0.28 μM inhibitor. It can be found that the deconvoluted XPS spectra of Fe $2p_{3/2}$ (as depicted in Figs. 8 and 9a) show four peaks. The peak at 709.2 eV was assigned to ferrous compound. The ferric compound appeared at 710.9 eV and the corresponding satellite peak occurred at 713.0 eV, while a peak of metallic Fe in the substrate emerged at 706.9 eV [11,40]. These results clearly reveal that the corrosion products covering the carbon steel surface are mainly composed of iron oxide and hydroxide either in the blank solution or the solution with inhibitor. This conclusion can also be verified from the O 1s XPS spectra presented in Figs. 8 and 9b, in which an $O^{2-}$ peak occurred at 530.6 eV. The peak of $OH^-$ appeared at 531.6 eV and the water molecule peak occurred at 533.2 eV [42,43]. The peak that originates from the inhibitor is probably included in the $OH^-$ peak because in general the O 1s peaks of organic compounds have been reported to appear at this energy position [11].

It is worth noticing that the depth profile of spectra of Cl in the blank solution (Fig. 8c) evidently shows that chloride ion was present not only on the surface of the film, but also within the film, and even at the film-substrate interface (sputtering time 730 s). Through further deconvolution of the Cl 2p spectrum after 10 s sputtering, as depicted in Fig. 8d, we can find two components. One that appeared at 199.5 eV can be attributed to $Cl^-$, and the other corresponding to $FeCl_x$ occurred at 201.1 eV [44]. These results reveal that a large number of $Cl^-$ was incorporated into the surface film during its formation in the blank solution. However, in the presence of the inhibitor, chloride ion was not detected either on the carbon steel surface or inside the surface film, as shown in Fig. 9c. These results suggest that the addition of the inhibitor effectively blocked the adsorption

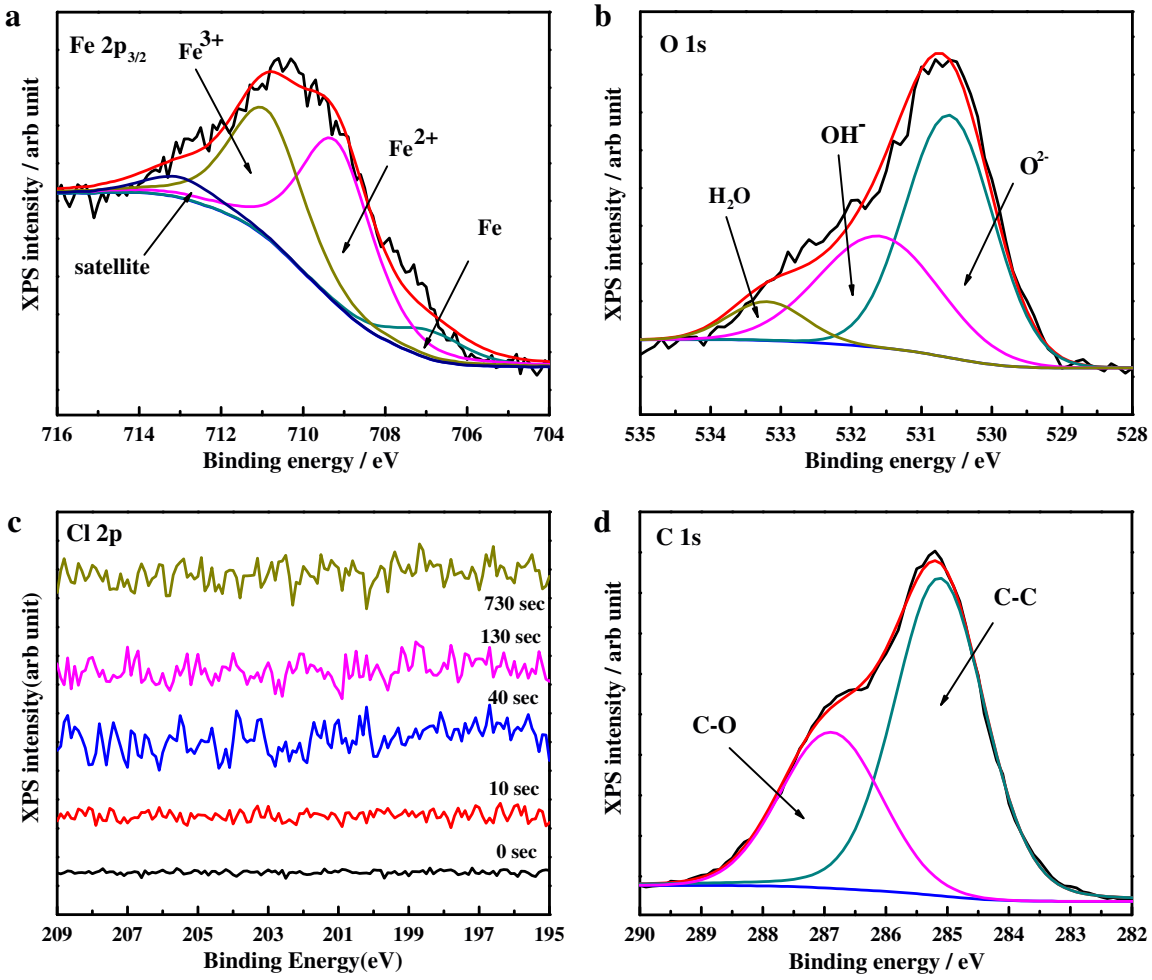


**Fig. 9.** XPS spectra for carbon steel samples immersed in 3.5% NaCl sat. $Ca(OH)_2$ solution with 0.28 μM inhibitor for 0.5 h at the OCP: (a) Fe $2p_{3/2}$; (b) O 1s; (c) the depth profile spectra of Cl 2p; (d) C 1s.

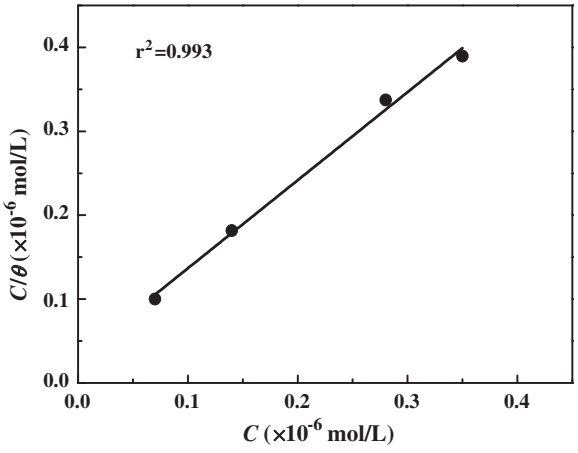


**Fig. 10.** Langmuir adsorption isotherm plot for carbon steel in 3.5% NaCl sat. $Ca(OH)_2$ solutions containing different concentrations of the inhibitor.

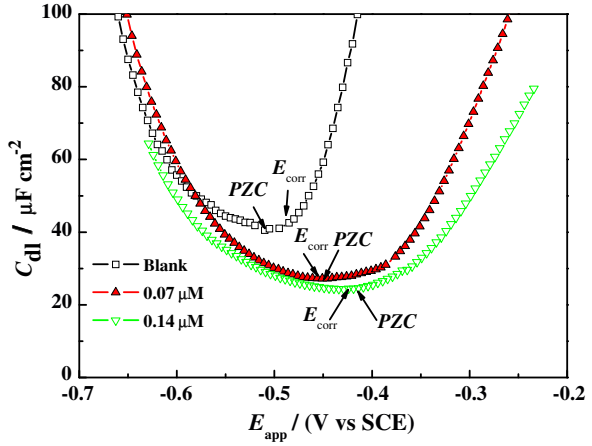


**Fig. 11.** The plots of $C_{dl}$ versus $E_{app}$ in 3.5% NaCl sat. $Ca(OH)_2$ solutions without and with different concentrations of the inhibitor.

of chloride ions onto the carbon steel surface via forming an adsorption protective layer on the metal surface and then suppressed the incorporation of chloride ions into the surface film. Hence, it can be concluded that the access of aggressive chloride ion to the carbon steel surface was entirely blocked by the adsorbed inhibitor molecules, thereby protecting the carbon steel against the attack of chloride ion and increasing its pitting potential [45].

The C 1s XPS spectrum shows a two-peak profile that is indicative of two chemical forms of C on the carbon steel surface (as depicted in Fig. 9d). The largest peak was assigned to the C—C bonds with a characteristic binding energy of 285.2 eV [46], whereas the other one can be attributed to the C—O (286.9 eV) bonds [47]. These facts confirm that the inhibitor is really present on the carbon steel surface. Hence, from XPS results it can be concluded that

**Table 3**
Values of PZC, $E_{corr}$ and $\varphi$ ($\varphi = E_{corr} - PZC$) recorded for carbon steel electrode in test solution without and with the addition of the inhibitor.

| Solution Conc. (μM) | PZC (mV/SCE) | $E_{corr}$ (mV/SCE) | $\varphi = E_{corr} - PZC$ (mV/SCE) |
|---|---|---|---|
| Blank | −511 | −486 | 25 |
| 0.07 | −451 | −462 | −11 |
| 0.14 | −429 | −434 | −15 |

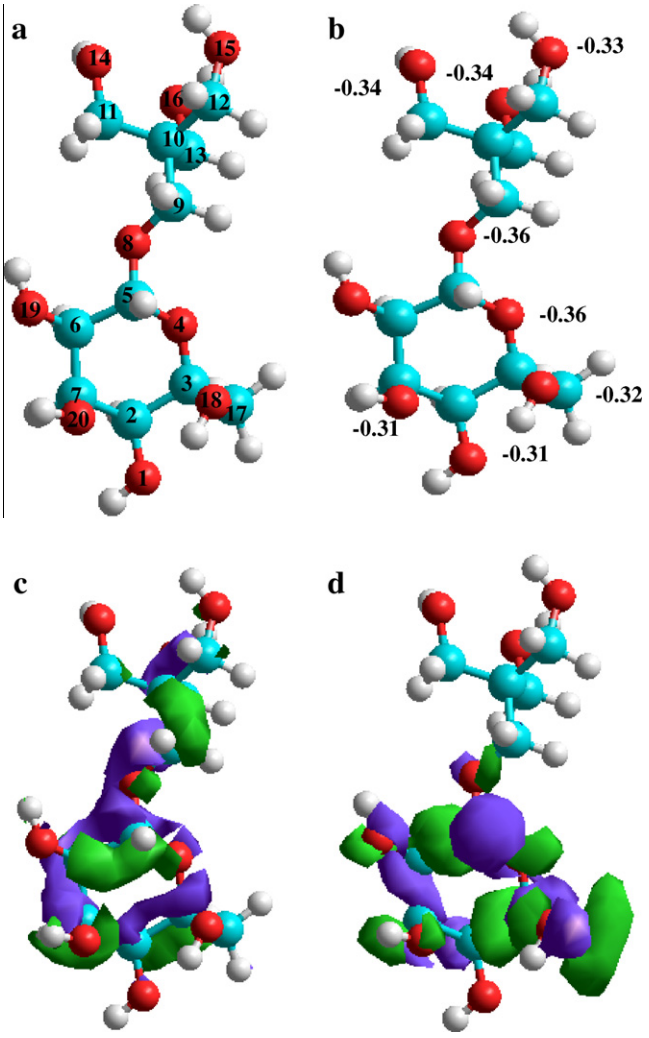


**Fig. 12.** Optimized molecular structure and the localization of molecular orbitals for the inhibitor: (a) optimized molecular structure; (b) the charges of the O atoms; (c) localization of HOMO orbitals; (d) localization of LUMO orbitals.

the adsorbed inhibitor molecules on the carbon steel surface can not only effectively hinder the adsorption of chloride ion onto the steel surface, but also prohibit chloride ion incorporation into the surface film by forming an adsorption protective layer.

### 3.3. Adsorption isotherm

The adsorption of inhibitor molecule on metal surfaces is a substitutional process, in which the adsorbed water molecules on metal surfaces are replaced by the inhibitor molecules. Several adsorption isotherms can be used to assess the adsorption behavior of such an inhibitor [48].

Temkin isotherm $$\exp(f\theta) = K_{ads}C \quad (2)$$

Langmuir isotherm $$\frac{\theta}{1-\theta} = K_{ads}C \quad (3)$$

Frumkin isotherm $$\frac{\theta}{1-\theta}\exp(-2f\theta) = K_{ads}C \quad (4)$$

Freundluich isotherm $$\theta = K_{ads}C \quad (5)$$

where $C$ is the inhibitor concentration, $f$ is the factor of energetic inhomogeneity, $K_{ads}$ is the adsorption equilibrium constant, and $\theta$ is the surface coverage for different inhibitor concentrations, which is the ratio of $\eta\%/100$ (see Table 2) [49–51].

For obtaining the best description of adsorption behavior of the inhibitor, all of the above adsorption isotherms were tested. The plot of $C/\theta$ versus $C$ yielded a straight line with a slope near to 1 and correlation coefficient 0.993, as shown in Fig. 10. This suggests that the adsorption of the PG inhibitor on the carbon steel surface obeys the Langmuir adsorption isotherm. Correspondingly, the $K_{ads}$ value can be calculated from the intercept of the straight line on the $C/\theta$ versus $C$ plot, and the related standard free energy of adsorption ($\Delta G^{\circ}_{ads}$) can be estimated by the following equation [49]:

$$K_{ads} = \frac{1}{55.5}\exp\left(-\frac{\Delta G^{\circ}_{ads}}{RT}\right) \quad (6)$$

where the value of 55.5 is the molar concentration of water in solution, $R$ is the universal gas constant, and $T$ is the absolute temperature.

The adsorption equilibrium constant ($K_{ads}$) obtained is $3.16 \times 10^7$ mol$^{-1}$ L. The high value of this $K_{ads}$ indicates that the inhibitor molecule possesses strong adsorption ability onto the carbon steel surface [52]. Generally, values of $\Delta G^{\circ}_{ads}$ around −20 kJ mol$^{-1}$ or lower are consistent with the electrostatic interaction between organic charged molecules and charged metal surfaces (physisorption); those around −40 kJ mol$^{-1}$ or higher involve electron sharing or transfer from organic molecule to the metal surface to form covalent bonds (chemisorption) [53]. The calculated $\Delta G^{\circ}_{ads}$ value is −52.7 kJ mol$^{-1}$, which means that the inhibitor's adsorption on the steel surface is typical of chemisorption [54].

### 3.4. Inhibition mechanism

The surface charge of a metal can be determined by comparison of its corrosion potential ($E_{corr}$) with respective the potential of zero charge (PZC), which plays an important role in the electrostatic adsorption process. Generally, the minimum value on the double layer capacitance ($C_{dl}$) versus applied potential ($E_{app}$) curve is the PZC value of the electrode; from that, the surface net charge of the metal in a given medium can be evaluated according to the difference $\varphi = E_{corr} - PZC$, where $\varphi$ is the Antropov's "rational" corrosion potential [55,56]. Fig. 11 shows the $C_{dl}$ versus $E_{app}$ plots for carbon steels tested after 0.5 h immersion in 3.5% NaCl saturated $Ca(OH)_2$ solutions in the absence and presence of an inhibitor. Table 3 lists the values of $E_{corr}$, PZC and $\varphi$. The positive value of $\varphi$ suggests that the carbon steel electrode surface is positively charged at its OCP in the blank solution [29,57]. This situation will initially favor the adsorption of negatively charged chloride ions onto the steel surface. The negative values of $\varphi$ in the inhibited solution could

be attributed to the adsorption of the inhibitor on the carbon steel surface. In this case, the adsorbed inhibitor molecules most likely formed a protective film on the steel surface and consequently acted as a barrier to hinder further mass and charge transference, thereby leading to an increase in its inhibition efficiency.

In addition to the above physical adsorption, a chemical adsorption can occur during the process of inhibitor adsorption on metal surfaces. In order to further confirm the adsorption mechanism, quantum chemical calculations were performed by Hyperchem7.5 with the semi-experience method [50]. The optimized molecular structure of the PG inhibitor and the Mulliken charges on oxygen atoms are shown in Fig. 12a and b, respectively. The molecular orbital distribution of HOMO (the highest occupied molecular orbital) and LUMO (the lowest unoccupied molecular orbital) of the inhibitor molecule are also respectively depicted in Fig. 12c and d. It can be seen that the HOMO was located over the entire molecule due to the presence of oxygen atoms in the inhibitor molecule, while the LUMO was mainly distributed on the moiety of a hemiacetal six-member ring. In addition, it can also be seen from Fig. 12b that the oxygen atoms in the inhibitor molecule carry negative charge centers. These calculation results reveal that the compound molecule can easily to form a coordinate bond through sharing the long-pair electrons on the oxygen atoms in the inhibitor molecule with the partly filled d-orbital of the iron atoms [58]. Among the discussed adsorption processes, physical adsorption must be the essential first step, which then allows for the strong chemical adsorption to take place.

## 4. Conclusions

(1) The inhibition efficiency and pitting potential on carbon steel in 3.5% NaCl saturated $Ca(OH)_2$ solution increase with increasing concentrations of a pentaerythritol glycoside inhibitor. The maximum inhibition efficiency of 89.8% was observed at 0.35 μM concentration.
(2) The compound acts as an anodic inhibitor through the forming of an adsorption protective film on the carbon steel surface, which can sufficiently hinder the access of chloride ion to the metal surface and suppress the chloride-induced corrosion in an alkaline solution.
(3) The adsorption of the inhibitor obeys the Langmuir adsorption isotherm via a strong chemical interaction with the carbon steel surface.
(4) Data obtained from electrochemical experiments along with quantum chemical calculations can give a reasonable interpretation about the inhibition mechanism of the inhibitor.

## Acknowledgements

The authors' gratefully acknowledge Dr. Weihua Li for her help in the quantum chemistry calculation and Professor Weitao Wu for English improving, and the financial support provided by the National Natural Science Foundation of China (Grant No. 51071161), the National Key Technology R&D Program (Grant No. 2007BAB27B03).

## References

[1] P. Garcés, P. Saura, A. Mendéz, E. Zornoza, C. Andrade, Corros. Sci. 50 (2008) 498–509.
[2] P. Ghods, O.B. Isgor, G.A. McRae, J. Li, G.P. Gu, Corros. Sci. 53 (2011) 946–954.
[3] N. Etteyeb, L. Dhouibi, H. Takenouti, M.C. Alonso, E. Triki, Electrochim. Acta 52 (2007) 7506–7512.
[4] F. Bolzoni, G. Fumagalli, L. Lazzari, M. Ormellese, M.P. Pedeferri, Mixed-in inhibitors for concrete structures, in: M. Raupach, B. Elsener, R. Polder, J. Mietz (Eds.), Corrosion of Reinforcement in Concrete: Mechanisms, Monitoring, Inhibitors and Rehabilitation Techniques, Woodhead Publishing Limited, Cambridge, England, 2007, pp. 185–202.
[5] M. Ormellese, M. Berra, F. Bolzoni, T. Pastore, Cem. Concr. Res. 36 (2006) 536–547.
[6] M. Ormellese, L. Lazzari, S. Goidanich, G. Fumagalli, A. Brenna, Corros. Sci. 51 (2009) 2959–2968.
[7] V.T. Ngala, C.L. Page, M.M. Page, Corros. Sci. 44 (2002) 2073–2087.
[8] H.E. Jamil, M.F. Montemor, R. Boulif, A. Shriri, M.G.S. Ferreira, Electrochim. Acta 48 (2003) 3509–3518.
[9] S. Sawada, C.L. Page, M.M. Page, Corros. Sci. 47 (2005) 2063–2078.
[10] L. Valek, S. Martinez, D. Mikulić, I. Brnardić, Corros. Sci. 50 (2008) 2705–2709.
[11] N. Nakayama, A. Obuchi, Corros. Sci. 45 (2003) 2075–2092.
[12] N. Nakayama, Corros. Sci. 42 (2000) 1897–1920.
[13] B. Elsener, M. Buchler, F. Stalder, H. Bohni, Corrosion 56 (2000) 727–732.
[14] S.F.U. Ahmed, H. Mihashi, Cem. Concr. Compos. 29 (2007) 365–376.
[15] X. Zhou, H. Yang, F. Wang, Electrochim. Acta 56 (2011) 4268–4275.
[16] A.B. da Silva, E. D'Elia, J.A.C.P. Gomes, Corros. Sci. 52 (2010) 788–793.
[17] A.R. Saliyan, A.V. Adhikari, Corros. Sci. 50 (2008) 55–61.
[18] S.K. Shukla, M.A. Quraishi, R. Prakash, Corros. Sci. 50 (2008) 2867–2872.
[19] G. Axci, Colloids Surf. A Physiconchem. Eng. Aspects 317 (2008) 730–736.
[20] K. Hill, O. Rhode, Fett-Lipid 101 (1999) 25–33.
[21] W. von Rybinski, K. Hill, Angew. Chem. Int. Ed. 37 (1998) 1328–1345.
[22] A.J.M. Valente, M. Nilsson, O. Söderman, J. Colloid Interface Sci. 281 (2005) 218–224.
[23] A. Capalbi, G. Gente, C. La Mesa, Colloids Surf. A Physicochem. Eng. Aspects 246 (2004) 99–108.
[24] M. Hato, Curr. Opin. Colloid Interface Sci. 6 (2001) 268–276.
[25] B. Hoffmann, G. Platz, Curr. Opin. Colloid Interface Sci. 6 (2001) 171–177.
[26] Kao Corporation, EP: 0 492 397 A1 (1992).
[27] A.K. Satapathy, G. Gunasekaran, S.C. Sahoo, Kumar Amit, P.V. Rodrigues, Corros. Sci. 51 (2009) 2848–2856.
[28] L.R. Chauhan, G. Gunasekaran, Corros. Sci. 49 (2007) 1143–1161.
[29] S. Martinez, L. Valek, I.S. Oslaković, J. Electrochem. Soc. 154 (2007) C671–C677.
[30] M. Yamaguchi, H. Nishihara, K. Aramaki, Corros. Sci. 36 (1994) 241–258.
[31] K. Aramaki, M. Tomihara, S. Furuya, M. Yamaguchi, H. Nishihara, Corros. Sci. 36 (1994) 1133–1141.
[32] K. Aramaki, M. Mizoguchi, H. Nishihara, J. Electrochem. Soc. 138 (1991) 394–398.
[33] F. Bentiss, M. Traisnel, M. Lagrenee, Corros. Sci. 42 (2000) 127–146.
[34] K. Jüttner, Electrochem. Acta 35 (1990) 1501–1508.
[35] S. Muralidharam, K.L.N. Phani, S. Pitchumani, S. Ravichadran, S.V.K. Lyer, J. Electrochem. Soc. 142 (1995) 1478–1483.
[36] M. Özcan, İ. Dehri, M. Erbil, Appl. Surf. Sci. 236 (2004) 155–164.
[37] F. Bentiss, M. Lagrenee, M. Traisnel, J.C. Hornez, Corros. Sci. 41 (1999) 789–803.
[38] L.J. Aljinovic, S. Gudic, M. Smith, J. Appl. Electrochem. 30 (2000) 973–979.
[39] A. Popova, E. Sokolova, S. Raicheva, M. Christov, Corros. Sci. 45 (2003) 33–58.
[40] M.M. Mennucci, E.P. Banczek, P.R.P. Rodrigues, I. Costa, Cem. Concr. Compos. 31 (2009) 418–424.
[41] P. Kern, D. Landolt, Electrochim. Acta 47 (2001) 589–598.
[42] K. Asami, K. Hashimoto, S. Shimodaira, Corros. Sci. 16 (1976) 35–45.
[43] L. Freire, X.R. Nóvoa, M.F. Montemor, M.J. Carmezim, Mater. Chem. Phys. 114 (2009) 962–972.
[44] O. Olivares-Xometl, N.V. Likhanova, M.A. Domínguez-Aguilar, J.M. Hallen, L.S. Zamudio, E. Arce, Appl. Surf. Sci. 252 (2006) 2139–2152.
[45] A. Ouerd, C. Alemany-Dumont, B. Normand, S. Szunerits, Electrochim. Acta 53 (2008) 4461–4469.
[46] M.S. Morad, J. Appl. Electrochem. 38 (2008) 1509–1518.
[47] J.I. Martins, T.C. Reis, M. Bazzaoui, E.A. Bazzaoui, L. Martins, Corros. Sci. 46 (2004) 2361–2381.
[48] J.M. Bastidas, P. Pinilla, E. Cano, J.L. Polo, S. Miguel, Corros. Sci. 45 (2003) 427–449.
[49] A.B. da Silva, E. D'Elia, J.A.C.P. Gomes, Corros. Sci. 52 (2010) 788–793.
[50] Y. Yan, W.H. Li, L.K. Cai, B.R. Hou, Electrochim. Acta 53 (2008) 5953–5960.
[51] R. Fuchs-Godec, Colloids Surf. A Physiconchem. Eng. Aspects 280 (2006) 130–139.
[52] S.A. Ali, H.A. Al-Mualllem, S.U. Rahman, M.T. Saeed, Corros. Sci. 50 (2008) 3070–3077.
[53] G. Moretti, F. Guidi, G. Grion, Corros. Sci. 46 (2004) 387–403.
[54] R. Hasanov, S. Bilge, S. Bilgic, G. Gece, Z. Kilic, Corros. Sci. 52 (2010) 984–990.
[55] M. Lagrenée, B. Mernari, M. Bouanis, M. Traisnel, F. Bentiss, Corros. Sci. 44 (2002) 573–588.
[56] Z.A. Chikh, D. Chebabe, A. Dermaj, N. Hajjaji, A. Srhiri, M.F. Montemor, M.G.S. Ferreira, A.C. Bastos, Corros. Sci. 47 (2005) 447–459.
[57] I. Sekine, Y. Nakahata, H. Tanabe, Corros. Sci. 28 (1998) 987–1001.
[58] K.F. Khaled, Electrochim. Acta 53 (2008) 3484–3492.